

Revealing Long-lived Electron-hole Migration in Core-Shell $\alpha/\gamma\text{-Fe}_2\text{O}_3/\text{FCP}$ for Efficient Photoelectrochemical Water Oxidation

Yinyin Li^a, Yifan Chen^c, Qiannan Wu^b, Rui Zhang^a, Mingjie Li^c, Yanhong Lin^a, Dejun Wang^a, and Tengfeng Xie^{a,*}

^a Institute of Physical Chemistry, College of Chemistry, Jilin University, Changchun 130012, P. R. China

^b State Key Laboratory of Inorganic Synthesis and Preparative Chemistry, College of Chemistry, Jilin University, Changchun 130012, P. R. China

^c Department of Applied Physics, The Hong Kong Polytechnic University, Hung Hom, Kowloon, Hong Kong, China

* Corresponding author: Tengfeng Xie

E-mail: xietf@jlu.edu.cn

List of Figures:

Fig. S1. The powder XRD patterns of $\gamma\text{-Fe}_2\text{O}_3/\alpha\text{-Fe}_2\text{O}_3$

Fig. S2. XPS survey spectra of $\gamma\text{-Fe}_2\text{O}_3/\alpha\text{-Fe}_2\text{O}_3/\text{FCP}$ and $\gamma\text{-Fe}_2\text{O}_3/\alpha\text{-Fe}_2\text{O}_3$.

Fig. S3. Raman spectra of $\gamma\text{-Fe}_2\text{O}_3/\alpha\text{-Fe}_2\text{O}_3$ and $\alpha\text{-Fe}_2\text{O}_3$.

Fig. S4. (a) SEM images of $\alpha\text{-Fe}_2\text{O}_3/\text{FCP}$. (b) EDS spectra of $\gamma\text{-Fe}_2\text{O}_3/\alpha\text{-Fe}_2\text{O}_3/\text{FCP}$.

Fig. S5. $\text{Ti-Fe}_2\text{O}_3$, $75\text{Ti-Fe}_2\text{O}_3/75\text{Ti-Fe}_2\text{O}_3$, $175\text{Ti-Fe}_2\text{O}_3/75\text{Ti-Fe}_2\text{O}_3$, and $225\text{Ti-Fe}_2\text{O}_3/75\text{Ti-Fe}_2\text{O}_3$: (a) Current density-potential curves; (b) ABPE spectra; (c) IPCE plots.

Fig. S6. LSV plots of $\gamma\text{-Fe}_2\text{O}_3/\alpha\text{-Fe}_2\text{O}_3/\text{FCP}$: (a) dipping times (2, 3, or 4) under 25° ; (b) dipping times (2, 3, 4, or 5) under 75° ; (c) dipping times (2, 3, 4, or 5) under 300° . (d) comparison under optimal conditions.

Fig. S7. LSV curves of phase junction measured without AM 1.5G irradiation.

Fig. S8. LSV plots of $\gamma\text{-Fe}_2\text{O}_3/\alpha\text{-Fe}_2\text{O}_3/\text{FCP}$ and $\gamma\text{-Fe}_2\text{O}_3/\alpha\text{-Fe}_2\text{O}_3/\text{CoPi}$ in KOH electrolyte

Fig. S9. (a) UV-vis absorption spectra of $\alpha\text{-Fe}_2\text{O}_3$ and phase junction. (b) Tauc's plots of $\alpha\text{-Fe}_2\text{O}_3$ and phase junction.

Fig. S10: Work Function measurement of pure $\alpha\text{-Fe}_2\text{O}_3$ and FCP.

Fig. S11. Equivalent circuit diagram and the fitted Nyquist plots for $\alpha\text{-Fe}_2\text{O}_3$ and phase junction.

Fig. S12. Experimental PL decay kinetics fitted under 485 nm: a) $\gamma\text{-Fe}_2\text{O}_3/\alpha\text{-Fe}_2\text{O}_3/\text{FCP}$, b) $\gamma\text{-Fe}_2\text{O}_3/\alpha\text{-Fe}_2\text{O}_3$, c) $\alpha\text{-Fe}_2\text{O}_3/\text{FCP}$, d) $\alpha\text{-Fe}_2\text{O}_3$.

Fig. S13. Pseudocolor TA plots of $\alpha\text{-Fe}_2\text{O}_3$ -based photoanodes under femtosecond laser pulses excitation with ~ 0.8 mJ fluence at 1 kHz repetition rate: a) $\gamma\text{-Fe}_2\text{O}_3/\alpha\text{-Fe}_2\text{O}_3/\text{FCP}$, b) $\gamma\text{-Fe}_2\text{O}_3/\alpha\text{-Fe}_2\text{O}_3$, c) $\alpha\text{-Fe}_2\text{O}_3/\text{FCP}$, d) $\alpha\text{-Fe}_2\text{O}_3$

List of Tables:

Table S1. The fitted results of Nyquist plots for $\alpha\text{-Fe}_2\text{O}_3$ and phase junction.

Table S2. Kinetic parameters of TAS decays of $\alpha\text{-Fe}_2\text{O}_3$ and phase junction under 400 nm excitation with time profiles of absorption probed at 580 nm.

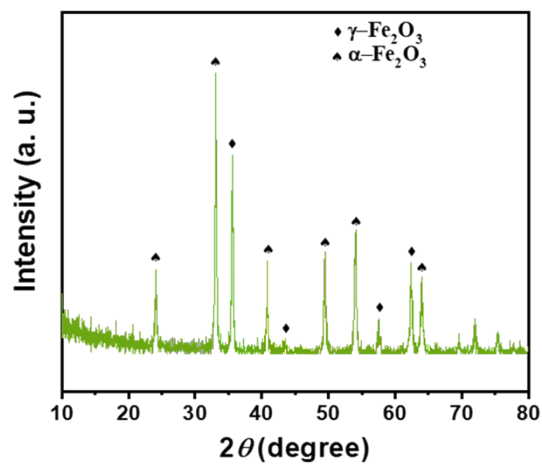


Fig. 1. (a) XRD patterns of $\gamma\text{-Fe}_2\text{O}_3/\alpha\text{-Fe}_2\text{O}_3$ powder.

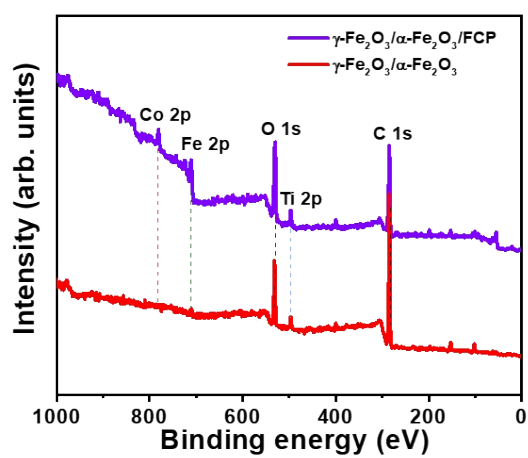


Fig. S2: XPS survey spectra of $\gamma\text{-Fe}_2\text{O}_3/\alpha\text{-Fe}_2\text{O}_3/\text{FCP}$ and $\gamma\text{-Fe}_2\text{O}_3/\alpha\text{-Fe}_2\text{O}_3$.¹

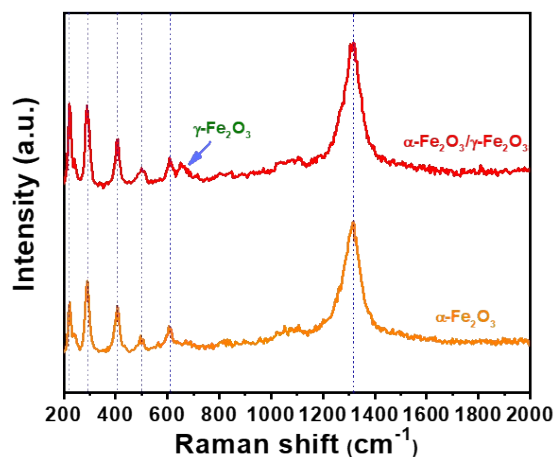


Fig. S3: Raman spectra of $\gamma\text{-Fe}_2\text{O}_3/\alpha\text{-Fe}_2\text{O}_3$ and $\alpha\text{-Fe}_2\text{O}_3$.

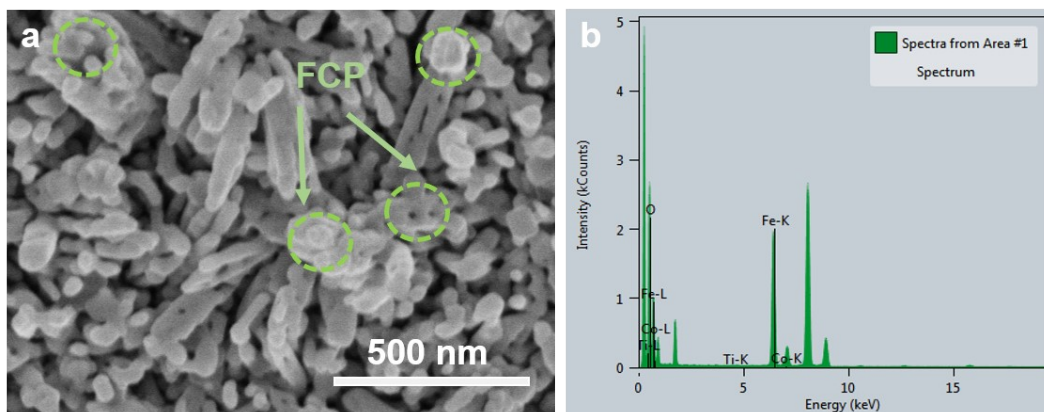


Fig. S4: (a) SEM images of $\alpha\text{-Fe}_2\text{O}_3/\text{FCP}$. (b) EDS spectra of $\gamma\text{-Fe}_2\text{O}_3/\alpha\text{-Fe}_2\text{O}_3/\text{FCP}$.

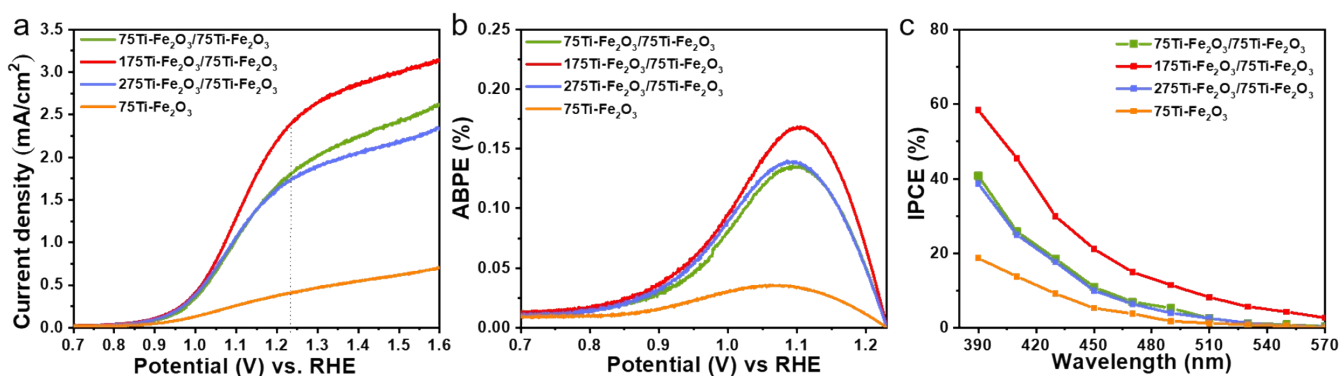


Fig. S5. $\text{Ti-Fe}_2\text{O}_3$, $75\text{Ti-Fe}_2\text{O}_3/75\text{Ti-Fe}_2\text{O}_3$, $175\text{Ti-Fe}_2\text{O}_3/75\text{Ti-Fe}_2\text{O}_3$, and $275\text{Ti-Fe}_2\text{O}_3/75\text{Ti-Fe}_2\text{O}_3$: (a) Current density-potential curves; (b) ABPE spectra; (c) IPCE plots.

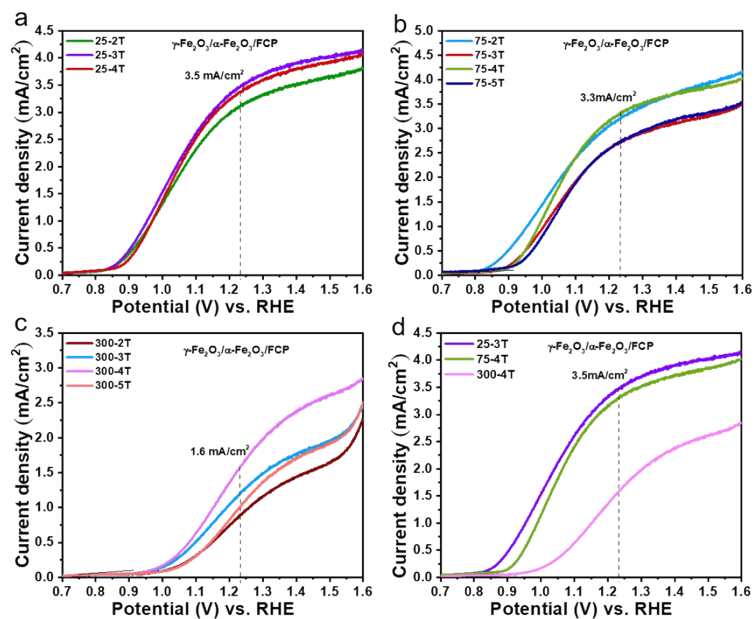


Fig. S6. LSV plots of $\gamma\text{-Fe}_2\text{O}_3/\alpha\text{-Fe}_2\text{O}_3/\text{FCP}$: (a) dipping times (2, 3, or 4) under 25°; (b) dipping times (2, 3, 4, or 5) under 75°; (c) dipping times (2, 3, 4, or 5) under 300°. (d) comparison under optimal conditions.²

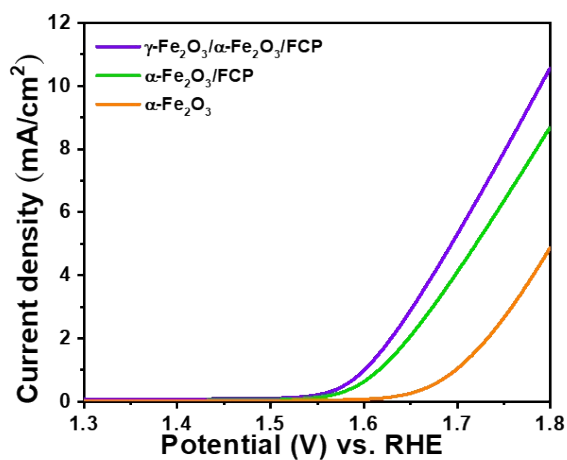


Fig. S7. LSV curves of $\alpha\text{-Fe}_2\text{O}_3$ and phase junction measured without AM 1.5G irradiation.

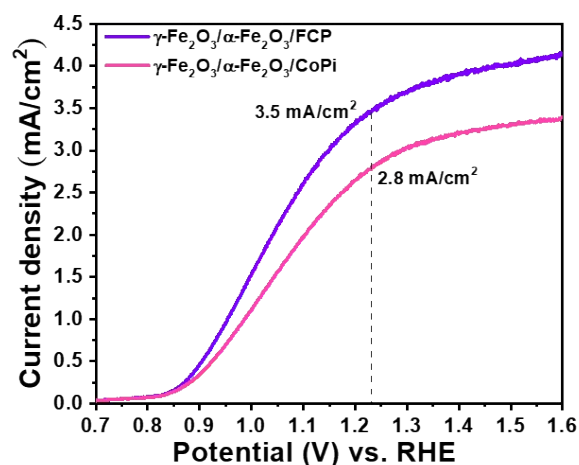


Fig. S8. LSV plots of $\gamma\text{-Fe}_2\text{O}_3/\alpha\text{-Fe}_2\text{O}_3/\text{FCP}$ and $\gamma\text{-Fe}_2\text{O}_3/\alpha\text{-Fe}_2\text{O}_3/\text{CoPi}$ in KOH electrolyte.

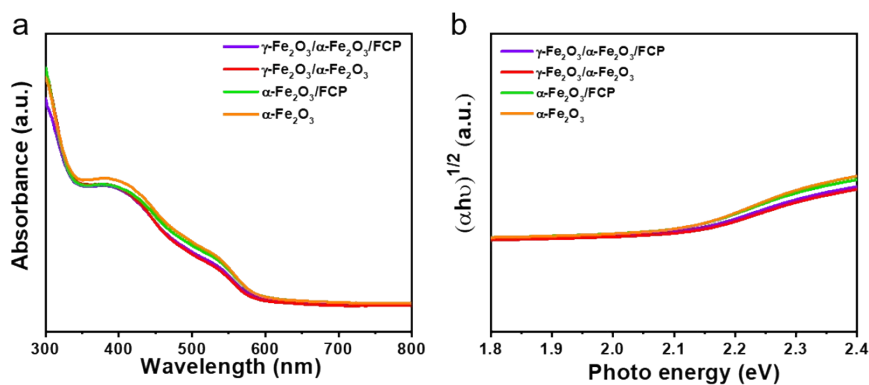


Fig. S9. (a) UV-vis absorption spectra of $\alpha\text{-Fe}_2\text{O}_3$ and phase junction. (b) Tauc's plots of $\alpha\text{-Fe}_2\text{O}_3$ and phase junction.

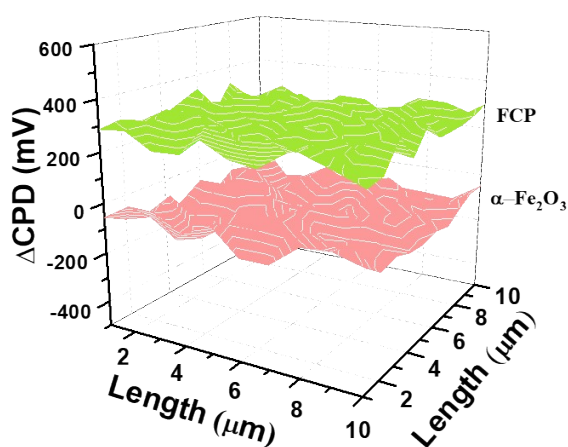


Fig. S10: Work Function measurement of pure $\alpha\text{-Fe}_2\text{O}_3$ and FCP.

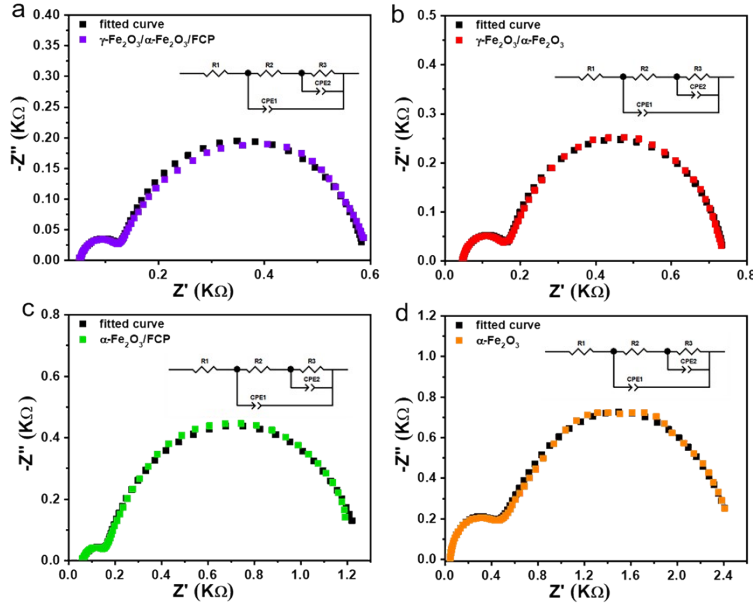


Fig. S11: Equivalent circuit diagram and the fitted Nyquist plots for $\alpha\text{-Fe}_2\text{O}_3$ and phase junction.

Samples	R_1 (Ω)	R_2 (Ω)	R_3 (Ω)
$\alpha\text{-Fe}_2\text{O}_3$	45.12	461.9	2036
$\alpha\text{-Fe}_2\text{O}_3/\text{FCP}$	61.74	129.9	1096
$\gamma\text{-Fe}_2\text{O}_3/\alpha\text{-Fe}_2\text{O}_3$	46.62	111.9	564.8
$\gamma\text{-Fe}_2\text{O}_3/\alpha\text{-Fe}_2\text{O}_3/\text{FCP}$	51.93	83.8	454.9

Table S1. The fitted results of Nyquist plots for $\alpha\text{-Fe}_2\text{O}_3$ and phase junction. Here, we named FeCo Prussian Blue as FCP.

In this work, the surface photovoltage (SPV) spectroscopic measurement was performed based on the system consisted of a lock-in amplifier (SR830-D SP) with a light chopper (SR540), a computer, a sample cell together with a source of monochromatic light provided by a 500 W xenon lamp (CHF-XM-500 W, Global Xenon Lamp Power) coupled with a grating monochromator (Omni-5007, Zolix). A low chopping frequency of 24 Hz was used. Before measurement, the system was calibrated by a DSI200 UV enhanced silicon detector to eliminate the possible phase

shift which was not correlated to the SPV response, so that any phase retardation reflected the kinetics of SPV response. The transient photovoltage (TPV) measurement was taken under a laser radiation pulse with the wavelength of 355 nm and pulse width of 5 ns from a third-harmonic Nd:YAG laser (Polaris II, New Wave128 Research, Inc.). The TPV signals were recorded by a 500 MHz digital phosphor oscilloscope (TDS 5054, Tektronix). Both SPV and TPV measurements are conducted in air at room temperature.

	A_1	τ_1 (ps)	A_2	τ_2 (ps)
α -Fe ₂ O ₃	0.81 ± 0.020	0.81 ± 0.019	0.22 ± 0.002	21.00 ± 0.58
α -Fe ₂ O ₃ /FCP	0.90 ± 0.011	0.80 ± 0.010	0.24 ± 0.002	29.59 ± 0.59
γ -Fe ₂ O ₃ / α -Fe ₂ O ₃	0.66 ± 0.009	0.94 ± 0.014	0.18 ± 0.001	33.45 ± 0.50
γ -Fe ₂ O ₃ / α -Fe ₂ O ₃ /FCP	0.56 ± 0.009	1.31 ± 0.029	0.18 ± 0.004	50.64 ± 0.78

Table S2. Kinetic parameters of TAS decays of α -Fe₂O₃ and phase junction under 400 nm excitation with time profiles of absorption probed at 580 nm.³ Here, we named FeCo Prussian Blue as FCP.

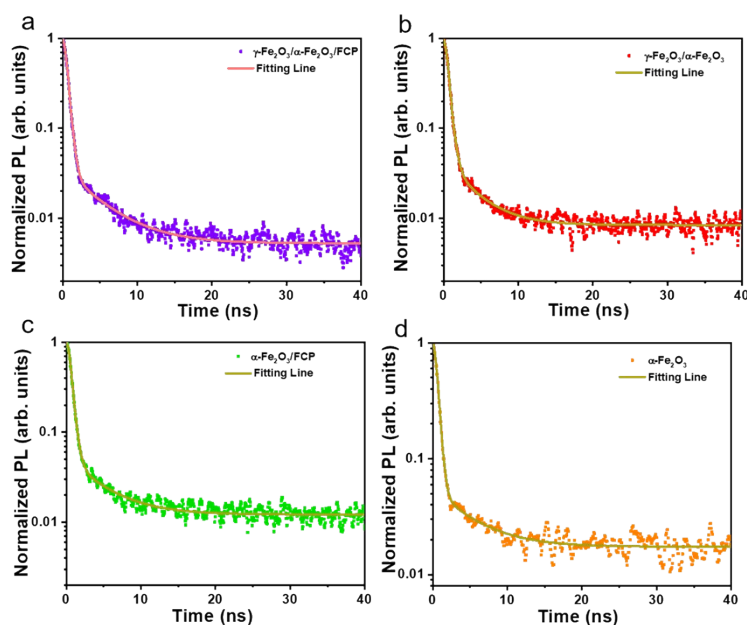


Fig. S12. Experimental decay kinetics fitted under 485 nm: a) γ -Fe₂O₃/ α -Fe₂O₃/FCP, b) γ -Fe₂O₃/ α -Fe₂O₃, c) α -Fe₂O₃/FCP, d) α -Fe₂O₃.

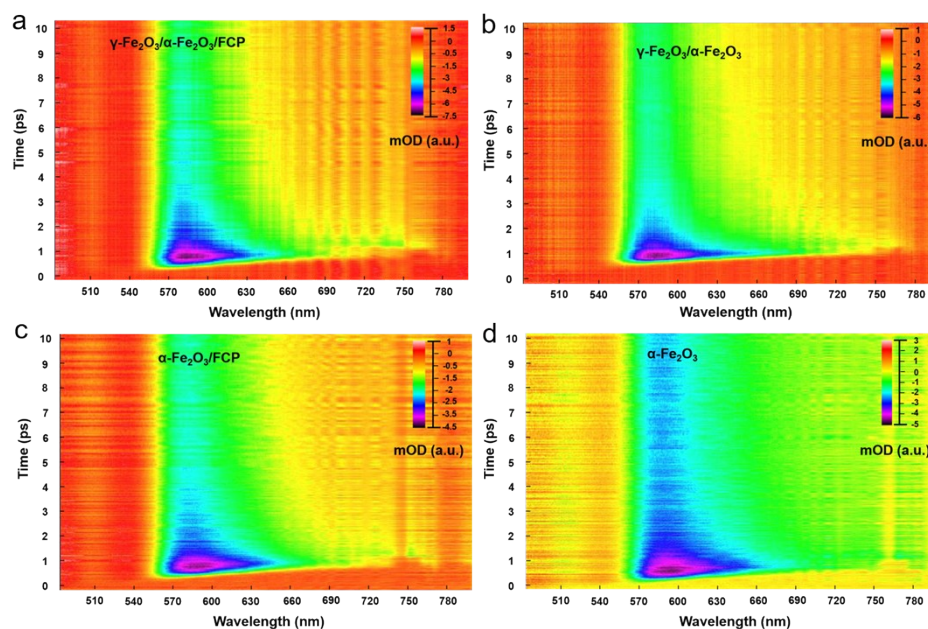


Fig. S13. Pseudocolor TA plots of α -Fe₂O₃-based photoanodes under femtosecond laser pulses excitation with ~ 0.8 mJ fluence at 1 kHz repetition rate: a) γ -Fe₂O₃/ α -Fe₂O₃/FCP, b) γ -Fe₂O₃/ α -Fe₂O₃, c) α -Fe₂O₃/FCP, d) α -Fe₂O₃.

Reference

1. S.-S. Yi, B.-R. Wulan, J.-M. Yan and Q. Jiang, *Adv. Funct. Mater.*, 2019, **29**, 1801902.
2. F. S. Hegner, I. Herraiz-Cardona, D. Cardenas-Morcoso, N. Lopez, J. R. Galan-Mascaros and S. Gimenez, *ACS Appl. Mater. Interfaces*, 2017, **9**, 37671-37681.
3. F. Liu, R. Shi, Z. Wang, Y. Weng, C. M. Che and Y. Chen, *Angew. Chem. Int. Ed.*, 2019, **58**, 11791-11795.